Internal Report
DESY M 07-02
November 2007

Wakes and Impedance Computations for The PETRA III Longitudinal Feedback Cavity

A.K. Bandyopadhyay[1], A. Jöstingmeier[1], A.S. Omar[1], and R. Wanzenberg[2]

[1]Department of Microwave and Communication Engineering,
Otto-von-Guericke University, Magdeburg, Germany

[2]Deutsches Elektronen-Synchrotron, DESY,
Hamburg, Germany

November, 2007

1 Introduction

At DESY the existing PETRA II storage ring will be converted into a 3rd generation synchrotron radiation source, called PETRA III. The total beam current in PETRA III can be limited by coupled bunch instabilities which are mainly driven by the parasitic modes of the RF cavities. Therefore, it has been planned to use longitudinal and transverse feedback systems to achieve the design current of 100 mA. A heavily loaded pillbox type cavity, based on the design of the DAFNE longitudinal feedback cavity, has been foreseen for the longitudinal feedback system of PETRA III. In order to dump all the coupled bunch instabilities, the cavity should have a maximum bandwidth of 125 MHz, which corresponds to the minimum bunch spacing foreseen for PETRA III (4 ns). Eight single cell feedback cavities will be installed into the PETRA III ring to damp the coupled bunch longitudinal phase oscillations. As these cavities can contribute significantly to the overall impedance of the machine, it is very important to compute the corresponding wakes and impedances. In this article analysis of the proposed longitudinal feedback cavity for PETRA III is presented in terms of wakes and impedances, possible higher order modes, shunt impedances and related topics.

2 Theory

2.1 Wakes and Impedances

In a particle accelerator, the charged particle beams travel inside a conducting pipe (beam pipe), inside which a very high vacuum is maintained. In practice, the beam encounters different cross sections of the beam pipe and interacts with them. The interaction of the beam with its surrounding are described in detail by the wakefields [1, 2]. From the wakefields several quantities, including the loss and kick parameters, can be calculated. The various loss

and kick parameters obtained in this way represent integral measures of the interaction of the beam with the considered part of the accelerator. In order to ensure proper operation of an accelerator and to achieve its design goals it is therefore required to know the wakefields of different parts of the accelerator.

Let us consider a point charge moving in free space at a velocity close to the velocity of light, c. With reference to the laboratory frame, the electric and magnetic fields of such a relativistic particle lie nearly in a plane which is perpendicular to its path. So, a second charge moving behind the first one on the same or on a parallel path, and at the same velocity $v \approx c$ will not be subjected to any forces from the fields produced by the leading charge. The situation is different if the two charges are moving in the vicinity of metallic objects or other boundary discontinuities. The trailing charge will still not experience the direct fields in the wavefront moving with the lead charge. This wavefront can, however, be scattered from the boundary discontinuities, and this scattered radiation will be able to reach the trailing charge and exert forces parallel and perpendicular to its direction of motion. These scattered waves are termed wakefields, and the integrated effects of these wakefields over a given path length of the trailing charge give rise to longitudinal and transverse wake potentials [3, 4].

Let us consider the situation shown in Fig. 1. Here, a test charge q_2 with momentum $\mathbf{p}$ is following a point charge q_1 along a discontinuity in the beam pipe. Both the charges have the same radial offset $\mathbf{r}$ from the axis and the test charge q_2 is at a distant s from q_1. The Lorentz force on the test charge due to the fields generated by the point charge q_1 is

$$\mathbf{F} = \frac{d\mathbf{p}}{dt} = q_2\,(\mathbf{E} + c\,\mathbf{e_z} \times \mathbf{B}), \tag{1}$$

where $\mathbf{p}$ denotes the momentum of the of the test charge q_2, $\mathbf{E}$ and $\mathbf{B}$ denote the electric and magnetic fields induced by the leading charge q_1 and $\mathbf{e_z}$ is the unit vector along the z-direction.

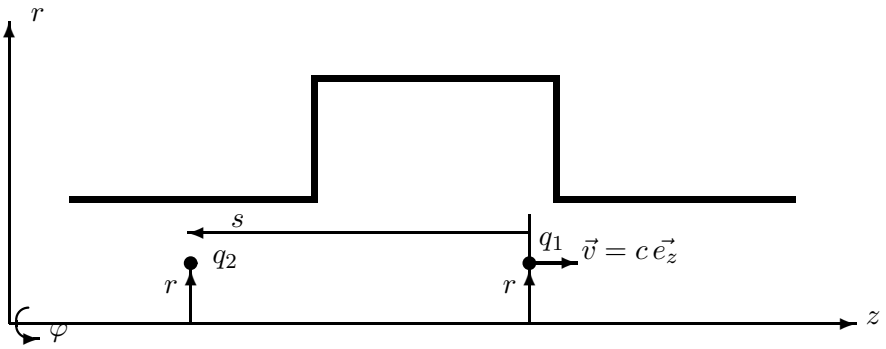

Figure 1: A point charge q_1 traversing a cavity with an offset r followed by a test charge q_2 with the same offset.

In this case, the wake potential due to the point charge q_1 can be defined as:

$$\mathbf{W}^{\delta}(r,s) = \frac{1}{q_1} \int_{-\infty}^{\infty} (\mathbf{E} + c\,\mathbf{e_z} \times \mathbf{B})_{t=(z+s)/c}\,dz, \tag{2}$$

assuming the position of the first particle is given by $z = ct$. The wake potential may be regarded as an average of the Lorentz force on a test charge. Causality requires $\mathbf{W}(s) = 0$ for $s < 0$. The distant s is positive in the direction opposite to the motion of the point charge q_1. The wake potential of a Gaussian bunch with charge density:

$$\rho(\mathbf{r}, t) = q_1 \ \lambda(z - ct), \qquad \lambda(s) = \frac{1}{\sigma\sqrt{2\pi}} \exp\left(-\frac{(s - s_0)^2}{2\,\sigma^2}\right)$$

is obtained by a convolution integral with the point charge wake potential $\mathbf{W}^\delta$

$$\mathbf{W}(r, s) = \int_0^\infty \lambda(s - s')\, \mathbf{W}^\delta(r, s')\, ds'. \tag{3}$$

The frequency domain description for the coupling between the beam and its environment can be obtained with the Fourier transform of the wake potential. The Fourier transform of the longitudinal wake potential is called the longitudinal impedance or the longitudinal coupling impedance

$$Z_\parallel(x, y, \omega) = \frac{1}{c} \int_{-\infty}^{\infty} W_\parallel(x, y, s) e^{-\frac{i\omega s}{c}}\, ds. \tag{4}$$

Similarly, the transverse impedance is defined as,

$$Z_\perp(x, y, \omega) = \frac{-i}{c} \int_{-\infty}^{\infty} W_\perp(x, y, s) e^{-\frac{i\omega s}{c}}\, ds. \tag{5}$$

The impedance spectra corresponding to a discontinuity along the beam pipe contains a number of peaks. The sharp peaks of the impedance spectra bellow the cut-off frequency of the beam pipe corresponds to the resonant modes of the discontinuity under consideration. Above the cut-off frequency of the beam pipe, a continuous spectrum corresponding to the beam pipe modes are usually seen. Although the impedances and wakes are the description of the same quantity connected by an integral transform, they are in general used to convey complementary information. The impedances are depicted up to a maximum frequency, whereas the wakes are depicted up to a finite time (or distance). Therefore, the impedance representation is more appropriate in depicting the long range phenomena, while the wake potential representation is appropriate to represent the short range one.

From the wake potential $\mathbf{W}(s)$ of a Gaussian bunch the following loss and kick parameters can be obtained:

$$k_\parallel = \int_{-\infty}^{\infty} W_\parallel(r = 0, s)\, \lambda(s)\, ds, \tag{6}$$

$$k_\parallel(1) = \int_{-\infty}^{\infty} W_\parallel(r = 0, s)\, \frac{d}{ds}\lambda(s)\, ds, \tag{7}$$

$$k_\perp = \frac{1}{r} \int_{-\infty}^{\infty} W_\perp(r, s)\, \lambda(s)\, ds. \tag{8}$$

If the total charge of the Gaussian bunch is q_1, the total energy loss of the bunch [5, 6] is given by,

$$\Delta W = q_1^2 \, k_{\parallel}. \tag{9}$$

The parameter $k_{\parallel}(1)$ is a crucial parameter for the longitudinal impedance model of the accelerator [7]. From the parameter $k_{\parallel}(1)$ and the kick parameter $k_{\perp}$ the coherent tune shifts of the lowest order bunch modes in the longitudinal ($\Delta\nu_s$) and transverse planes ($\Delta\nu_\beta$) can be calculated according to the following equations [8, 7]:

$$\Delta\nu_s = \nu_s \frac{I_B \, R \, T_0}{2 \, h \, U_{\rm rf}} \, k_{\parallel}(1), \tag{10}$$

$$\Delta\nu_\beta = \frac{I_B \; < \beta > \; T_0}{4\pi \, E/e} k_{\perp}, \tag{11}$$

where ν_s is the synchrotron tune, I_B the single bunch current, R the average radius, T_0 the revolution time, h the harmonic number, $U_{\rm rf}$ the total RF voltage, $< \beta >$ the average beta-function and E the energy of the accelerator.

2.2 Modal analysis and different cavity parameters

To compute the possible losses and kicks due to a particular resonant mode of the part under consideration, an eigenmode analysis is used. The computer codes like URMEL [9], Microwave studio (MWST) [10], MAFIA [11] etc. are generally used for this purpose. After an eigenmode analysis of the structure under analysis, the components of electric and magnetic fields due to computed eigenmodes can be obtained from the solver. From the numerically calculated fields the longitudinal voltage (V_L) due to a mode with angular resonant frequency ω can be obtained as

$$V_L(r) = \int_0^L E_z(r,z) \, \exp(-\frac{i\omega z}{c}) \, dz, \tag{12}$$

where E_z is the longitudinal component of the electric field. The total stored energy in the mode (considering the symmetries and time averaging) can be calculated as

$$U = \frac{\epsilon_0}{4} \int |\mathbf{E}|^2 \; d^3r \tag{13}$$

From the voltage and stored energy the modal loss parameter and the ratio of the shunt impedance and quality factor (R/Q) can be obtained. These parameters are usually calculated using the post processor module of the computer codes (e.g. MAFIA). The loss parameter ($k(r)$) and the R/Q value are calculated as:

$$\begin{aligned} k(r) &= \frac{|V_L(r)|^2}{4\,U} \\ \frac{R(r)}{Q} &= \frac{2 \; k(r)}{\omega} \end{aligned} \tag{14}$$

It may be noted here that a particle bunch with charge q traversing the cavity with radial offset r will lose the energy $q^2\ k^{(n)}(r)$ into the nth mode of the cavity.

It is important to know the power P_{sur} dissipated at the inner cavity due to the surface resistivity R_{sur}. The dissipated power into the surface can be calculated from the tangential magnetic field:

$$P_{sur} = \frac{1}{2}\ R_{sur}\ \int |H_\phi|^2\ dA. \tag{15}$$

The power which is dissipated into the cavity surface can also be characterized by the quality factor Q or the parameter G_1 [12]. The parameter G_1 is defined as the product of the quality factor of the mode and the surface resistance of the cavity wall. These parameters can be computed as,

$$Q = \frac{\omega\ U}{P_{sur}} \tag{16}$$

$$G_1 = R_{sur}\ Q. \tag{17}$$

2.3 Methods for wakefield and Impedance computations

2.3.1 Using MAFIA for wakefield computations

MAFIA is a well known three dimensional electromagnetic field simulator, widely used by the accelerator community. In the first step for wake computation with MAFIA, the geometry under consideration is modeled using the mesh generator. Afterwards the two dimensional eigenmode solver is used to compute the eigenmodes corresponding to the waveguide ports. These modes are then loaded in the MAFIA time domain solver module for proper terminations of the waveguide ports during the time domain computations. Afterwards the beam-properties (the beam width, total charge of the beam, orientation of the beam etc.) are specified and the time domain solver is started for an appropriate time range. Usually the minimum time range is taken equal to the time the beam takes to traverse the whole structure under consideration. However, it is often required to use a longer time range in order to compute the long range wakes or to obtain a fine frequency resolution in the corresponding impedance spectrum. Once the computations are finished, the results are exported and further processed with MATLAB [13] for extracting different loss- and kick- parameters. These post processing tasks can also be done using the post-processor module of MAFIA.

2.3.2 Off-axis wake computations

Computation of the wakes due to an off-axis beam usually requires at least double of the memory required to compute the wakes due to an on-axis beam (for axially symmetric structures). This is because although the structure remains geometrically symmetric in both cases, it becomes asymmetric with respect to the exciting off-axis beam. Due to this reason, in many instances the available computer memory become the limiting factor for the time domain off-axis wake computations. This problem is more severe in case of large structures, containing small geometrical details. In order to represent the small geometrical details correctly, a fine

meshing is required. As for the wake computations (with MAFIA) one needs an equidistant mesh distribution in the direction of the beam, this leads to a huge number of mesh cells. In these situations, it would be very useful if only a part (say one-quarter or one-half, depending upon the symmetry of the considered structure) of the geometry is modeled and the wake computation results of some combinations of different boundary conditions are obtained. Afterwards the results could be combined to get the response of the whole structure. In this way, the memory requirement is halved at the cost of computational time.

To test the validity and accuracy of this method, off-axis wake computations for very simple and small structures can be considered. At the first step two sets of wakefield computations could be done considering an off-axis beam (say, y-offset) and one quarter of the structure. The boundary conditions for the wake computations for the quarter geometry is tabulated in Table 1. Then the results are combined to obtain the actual wakes for the beam with y-offset. It can be noted here that for the first set of the boundary conditions, we can consider the computed wakefields W_{qew} generated by the current (I) and its image current (-I) (as an electric wall has been used at the y-min boundary). Similarly, for the second set of boundary conditions (magnetic wall at the y-min boundary), the computed wakefields (W_{qmw}) were due to (I) and its image current (I). As the wakefield computations involve only linear operations, the results corresponding the excitation (I) should be simply given by $\frac{W_{qew}+W_{qmw}}{2}$.

For the verification, the off-axis wakes can be computed directly for half of the structure with the boundary conditions shown in Table 2. As the structure is symmetric with respect to the yz-plane, a magnetic wall has been used along x-min (x = 0). The errors in computed wakes between both the methods should be very small.

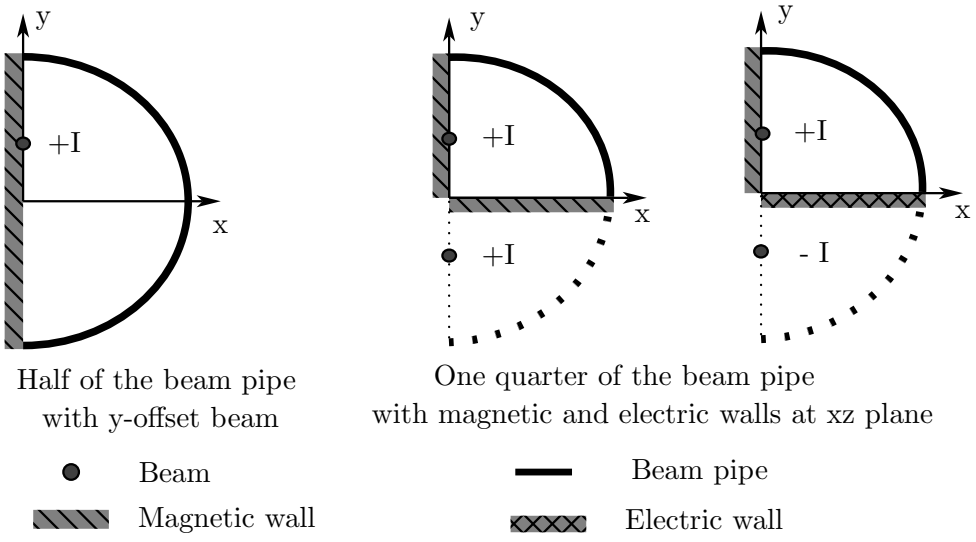

Figure 2: Schematic diagram depicting the excitations and boundary conditions for off-axis wake computations considering one half and one quarter of the beam pipe.

Two simple test geometries have been considered to demonstrate the suggested method. The first geometry is a simple pill-box cavity along the beam pipe, while the other geometry

boundary	Boundary condition
x-min, x-max	Magnetic (Magnetic), Electric (Electric)
y-min, y-max	Electric (Magnetic), Electric (Electric)
z-min, z-max	Waveguide(Waveguide), Waveguide (Waveguide)

Table 1: Boundary conditions used in MAFIA for the time domain wakefield computations for one quarter of the test structure.

boundary	Boundary condition
x-min, x-max	Magnetic, Electric
y-min, y-max	Electric, Electric
z-min, z-max	Waveguide, Waveguide

Table 2: Boundary conditions used in MAFIA for the time domain wakefield computations for half of the test structure.

contains cylindrical holes in the upper part and lower parts of the beam pipe. The first test structure can be considered as representative of the cases where a cavity is inserted along the beam pipe (i.e. the RF cavities, kickers etc.). In these situations usually a stong wakes is expected. The other structure is representative of the situations where small discontinuities are present in the beam pipe (BPMs, small transitions etc.). The MAFIA models of both test geometries are shown in Fig. 3. The hole in the upper part of the beam pipe can be seen in Fig. 3(b), while that in the lower part of the beam pipe is not visible.

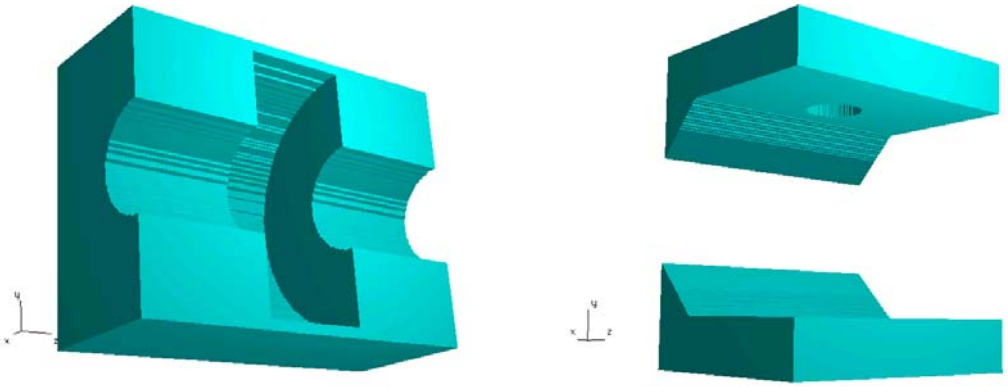

(a) Half of the test structure geometry with pillbox cavity.

(b) Half of the test structure geometry with holes in the upper and lower wall of the beam pipe.

Figure 3: One half of the geometries considered as the test structures.

The comparison between the computed longitudinal wakefields for the test structure are

shown in Fig. 4(a). Once the longitudinal wake was computed using one quarter of the first test structure (combining results of two different boundary conditions) and once it was computed directly using half structure. The absolute percentage error normalized to the maximum is shown in Fig. 4(b). Fig. 5 shows the comparison of the transverse wake and the corresponding absolute percentage error (normalized to the maximum).

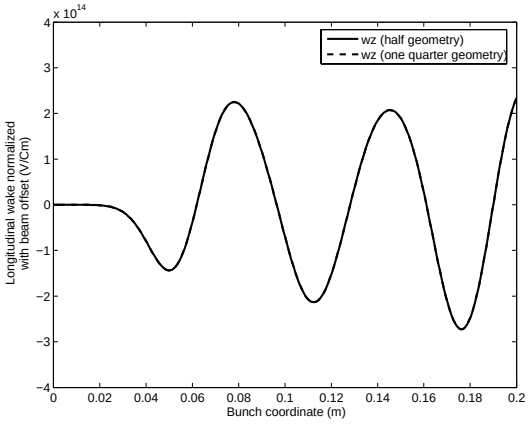

(a) Comparison between the longitudinal component of wake computed considering one half and one quarter of the first test geometry.

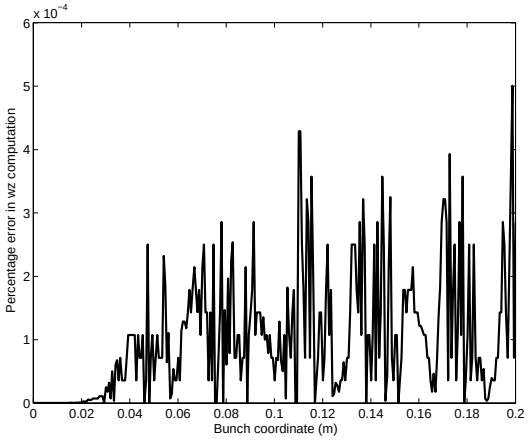

(b) Absolute percentage error (normalized to the maximum) in longitudinal wake computation.

Figure 4: Comparison of computed longitudinal wake for the first test geometry and absolute percentage error.

The wake computation results for the second structure are shown in Figs. 6 and 7. The absolute percentage errors normalized to the corresponding maximum values are also shown. From the figures it is clear that in this case the percentage error in transverse wake computation is much higher than that of the longitudinal component. One possible reason for this may be the difference in computing the transverse wakes considering one half of a structure and one quarter of the same structure. The error is less than 1% in case of longitudinal wake computations whereas it is below than 10% in case of transverse wake computations.

2.3.3 Forward and backward wave shunt impedance computation

For the shunt impedance computations, the MAFIA T3 module has been used. A Gaussian beam suitable to excite the feedback cavity in the operating frequency band has been considered as the excitation signal. The excitation signal has been fed to the cavity through one of the coaxial ports. In order to compute the shunt impedance, one needs to obtain the accelerating voltage along the cavity axis corresponding to this excitation. This accelerating voltage (V_{acc}) can be computed by integrating the longitudinal electric field (corresponding to the coaxial excitation) along the cavity length. In MAFIA, the wake integration monitor computes the wake integral according to equations 2 and 3. The orientation of the second term of the integral of equation 2 (i.e. $c\,\mathbf{e_z} \times \mathbf{B}$) lies in the transverse plane. Therefore, this term

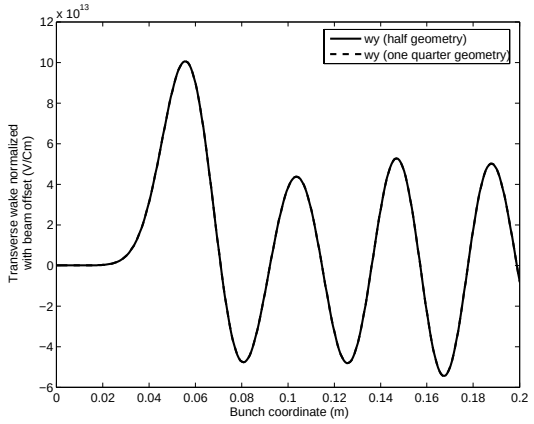

(a) Comparison between the transverse component of wake computed considering one half and one quarter of the first test geometry.

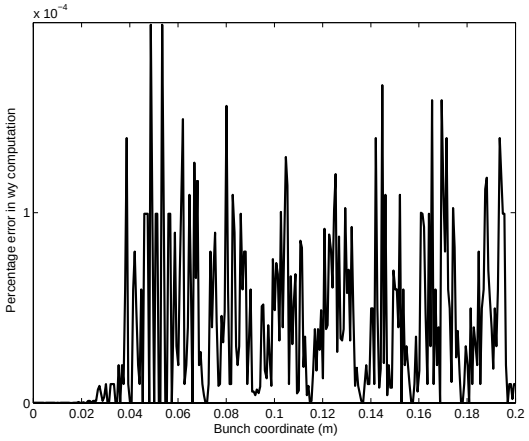

(b) Absolute percentage error (normalized to the maximum) in transverse wake computation.

Figure 5: Comparison of computed transverse wake for the first test geometry and absolute percentage error.

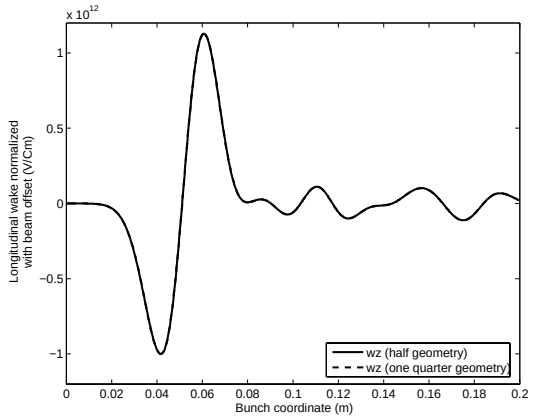

(a) Comparison between the longitudinal component of wake computed considering one half and one quarter of the second test geometry.

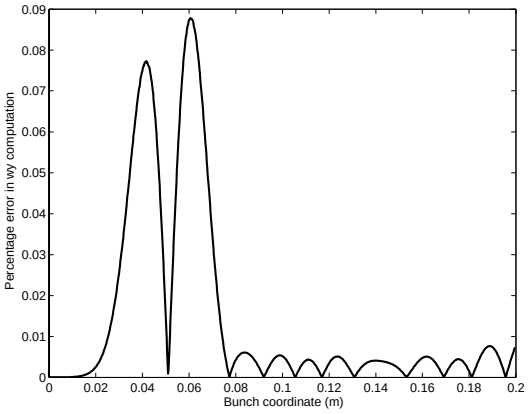

(b) Absolute percentage error (normalized to the maximum) in longitudinal wake computation.

Figure 6: Comparison of computed longitudinal wake for the second test geometry and absolute percentage error.

does not contribute to the longitudinal component of the integral. So, a wakefield monitor along the path of the beam can be used to compute the accelerating voltage (V_{acc}) due to the excitation through the coaxial port. In order to activate the wakefield monitor, at first a beam with non-zero charge can be considered. Just before the time domain computational run, the charge of the beam is set equal to zero, so that the computed acceleration voltage is entirely due to the excitation through the coaxial port. To compute the accelerating voltage

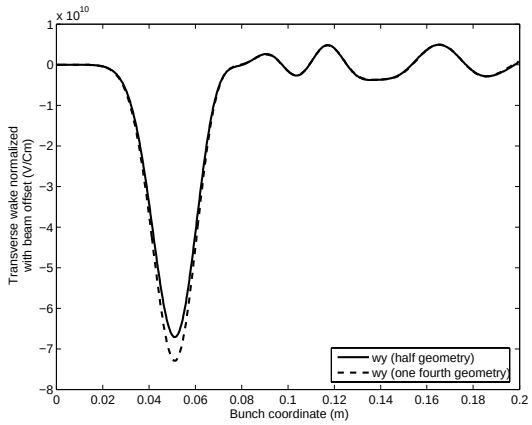

(a) Comparison between the transverse component of wake computed considering half of the geometry and quarter of the geometry.

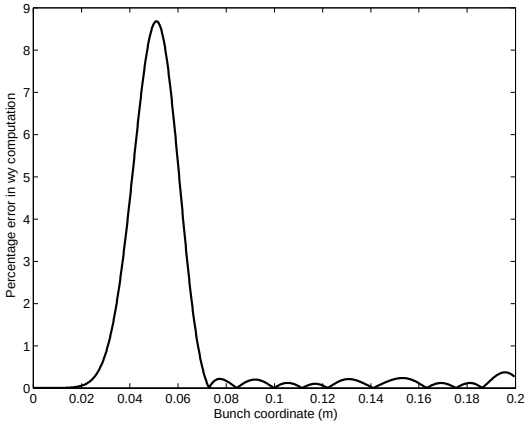

(b) Absolute percentage error (normalized to the maximum) in transverse wake computation.

Figure 7: Comparison of computed transverse wake for the second test geometry and absolute percentage error.

along the axis of the cavity, the wakefield monitor is set at $x = 0,\ y = 0$. Afterwards, a Fourier transform is used to convert all the time domain data into the frequency domain. For our simulations, the waveguide ports at both the ends of the beam pipe as well as the coaxial ports have been terminated with their corresponding wave impedances. All the outgoing wave amplitudes have been recorded at the coaxial ports. Two sets of computation runs have been done, one for the forward wave case and the other one is for the backward wave case. The shunt impedance (R_s) can be computed according to the equation,

$$R_s = \frac{\mid V_{acc} \mid^2}{2\, P_{in}}, \tag{18}$$

where P_{in} is the input power fed into the cavity through the coaxial ports.

3 Studies of the PETRA III longitudinal feedback cavity

3.1 PETRA III longitudinal feedback cavity

The PETRA III synchrotron radiation facility will be operating in a multibunch mode. Multibunch operations of the accelerators are usually affected by several instabilities which can considerably limit the desired beam current. The coupled bunch instabilities are among those instabilities which are severe constraints to achieve the desired beam current and shape.

Employment of active bunch by bunch feedback system is one of the most effective measures to dump coupled bunch instabilities. In these feedback systems, the deviations of bunches from their reference positions are measured and a correction signal is created based on the measured deviation. Afterwards, the correction signal is amplified and applied to the particle bunches.

The amplified correction signal is applied to the particle bunches by means of the feedback cavities or 'kickers'. Both longitudinal and transverse kickers are usually employed to deliver the appropriate component of kick. Several designs for the longitudinal feedback kickers exist, which includes the coaxial drift tube based design (ALS, PLS, PEP-II) [14], overdamped cavity based design (DAFNE, BESSY II, KEKB)[15], pill-box cavity with striplines (SRRC, TLS) [16]. Among the designs mentioned above, the overdamped cavity based design is widely used and is planned to be used for PETRA III. The longitudinal feedback cavity of PETRA III is

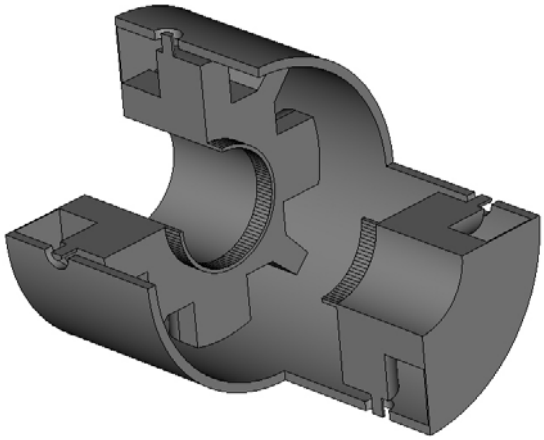

Figure 8: A cut view of the PETRA III longitudinal feedback cavity with nose cones.

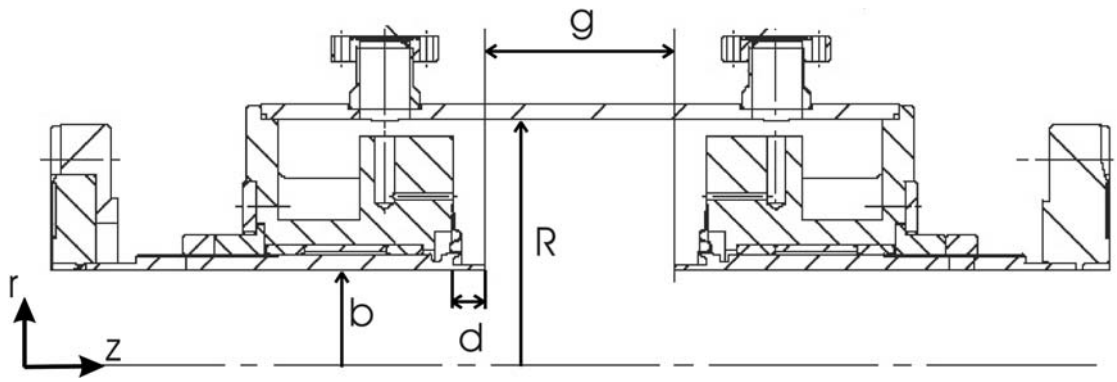

Figure 9: Part of a technical drawing of the PETRA III longitudinal feedback cavity with nose cones. The basic dimensions of the cavity are b = 30 mm, R = 77.8 mm, g = 60 mm and d = 10 mm.

basically a heavily loaded pillbox cavity. It has eight coaxial ports for connection to the driving amplifiers (input ports) and the dummy loads (output ports). A cut view of a longitudinal feedback cavity is shown in Fig. 8. The basic dimensions of the cavity are shown in Fig. 9. A high shunt impedance (the ratio between the square of the kick voltage seen by the beam and

the peak forward power at the input) and high bandwidth are usually the desired parameters for an efficient feedback cavity. It is known that in order to dump all of the coupled bunch instabilities, the required maximum bandwidth is $(f_{RF}/2)$, considering all the buckets filled. For a different filling mode, the bandwidth requirement will be different, depending upon the spacing between the bunches. For PETRA III, the maximum required bandwidth is 125 MHz, corresponding to a bunch spacing of 4 ns [8]. The high bandwidth of the cavity is achieved by strongly loading it with the special ridged waveguides which can be connected to the external loads.

3.2 Eigenmode analysis

The eigenmode solvers of MWST and MAFIA have been used to compute the resonant frequencies of the feedback cavity. The mesh views at two different planes of the cavity are shown in Fig. 10. The resonant frequencies of the first 14 modes (according to the boundary conditions of Table 4), the modal loss parameters at zero offset and the quality factors computed with MAFIA are shown in Table 4. From the table, it can be seen that the resonant frequency of the TM_{010} like mode, which is to be used for the beam correction, is 1.3079 GHz with a quality factor of 10579 (copper). The electric field distribution for this mode is shown in Fig. 11. It can be noted that the resonant frequency of the operating TM_{010} mode without the nose cones comes out to be 1.398 GHz (1.392 GHz from MWST). Therefore, the inclusion of the nose cones have lowered the resonant frequency of the operating mode. This may be of particular interest as there is a plan to use the nose cones for cavity tuning. From Table 4 it can be noticed that below the cutoff frequency of the beam pipe (2.93 GHz for the TE Modes and 3.82 GHz for the TM modes) the resonant modes at frequencies 1.7692, 2.0782 and 2.4906 GHz are having high loss factors. The details of the electric field distributions of these modes are shown in Figs. 12, 13 and 14, respectively. The conductivity of copper has been taken as $5.8 \times 10^7\,(\Omega\, m)^{-1}$ for the computations. As can be noticed from the figures the electric field distribution is strong around the ridges of the waveguide and have a relatively weak distribution around the beam pipe for the modes near 1.77 GHz and 2.08 GHz.

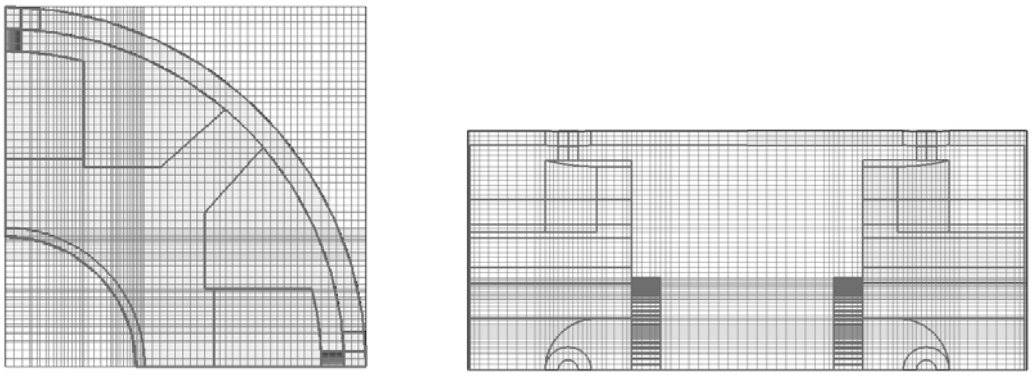

(a) Mesh view at a transverse plane.

(b) Mesh view at a longitudinal plane.

Figure 10: Mesh view at two planes for the feedback cavity.

Boundaries	Boundary conditions
x-min, x-max	Magnetic, Electric
y-min, y-max	Magnetic, Electric
z-min, z-max	Magnetic, Magnetic

Table 3: Boundary conditions used for the eigenmode computations with MAFIA.

To compute the other resonant modes, MAFIA simulations with different boundary conditions at the x-min and y-min boundary have been used. The corresponding results have been verified by a microwave studio simulation with the full geometry of the feedback cavity. The resonant frequencies of all the modes bellow the cutoff frequency of the beam pipe are listed in the Table 5. The computed resonant frequencies agree within 1 percent relative difference. For the MAFIA simulations a manual meshing scheme with diagonal filing have been used whereas for the MWST simulations the 'partially filled cells' and automesh facilities have been used. These differences in meshing is most probably the cause for the slight differences between the computed resonant frequencies.

Mode No.	Frequency (GHz)	Quality factor	Loss Parameter (offset = 0) [V/(p C)]
1	1.3079	10579	3.39×10^{-1}
2	1.7692	4619	1.87×10^{-2}
3	1.9281	4236	5.17×10^{-10}
4	1.9885	4151	2.82×10^{-9}
5	2.0782	4730	3.59×10^{-2}
6	2.4906	9604	7.69×10^{-2}
7	2.7216	17380	2.09×10^{-11}
8	3.1752	23884	1.77×10^{-12}
9	3.4582	26473	1.23×10^{-3}
10	3.6513	14719	2.76×10^{-11}
11	3.7201	22717	3.69×10^{-4}
12	3.8162	16699	1.37×10^{-2}
13	3.8610	13901	5.93×10^{-3}
14	4.0116	11485	1.03×10^{-10}

Table 4: The resonant frequencies, quality factors (copper) and modal loss parameters for the first 14 modes of the longitudinal feedback cavity. The corresponding boundary conditions are shown in Table 3.

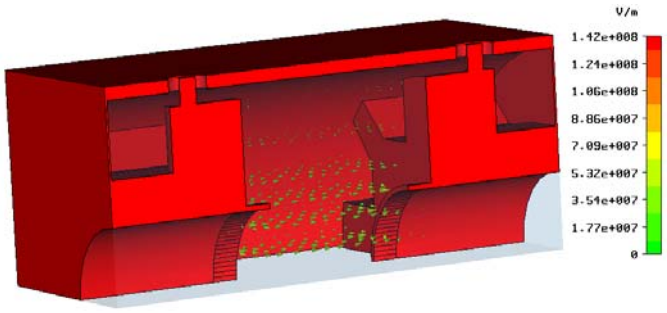

Figure 11: Electric field distribution of the operating TM_{010} like mode of the longitudinal feedback cavity with nose cones (resonant frequency 1.3079 GHz).

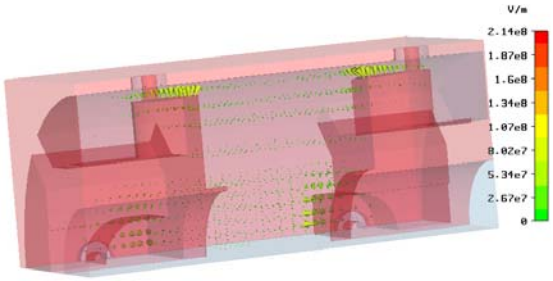

(a) Three dimensional electric field distribution of the mode near 1.77 GHz.

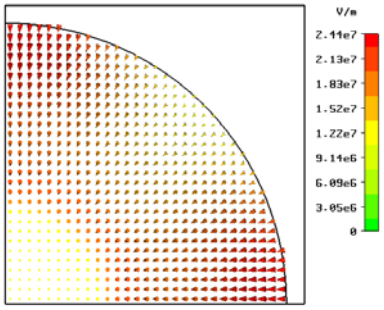

(b) Two dimensional projection of the electric field at a transverse plane.

Figure 12: The electric field distribution of the mode no. 2 (table 4) with resonant frequency 1.7692 GHz.

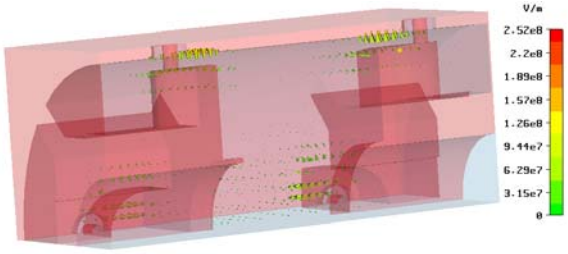

(a) Three dimensional electric field distribution of the mode near 2.08 GHz.

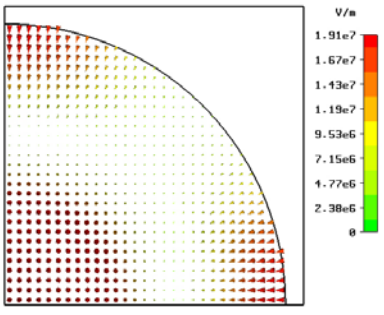

(b) Two dimensional projection of the electric field at a transverse plane.

Figure 13: The electric field distribution of the mode no. 5 (table 4) with resonant frequency 2.0782 GHz.

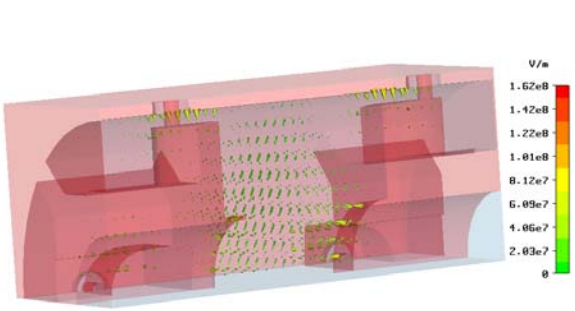

(a) Three dimensional electric field distribution of the mode near 2.49 GHz.

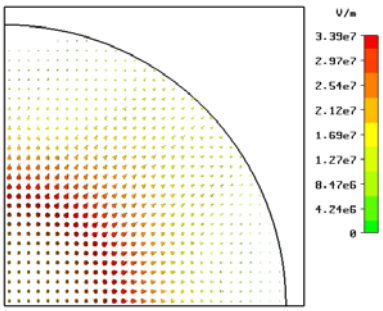

(b) Two dimensional projection of the electric field at a transverse plane.

Figure 14: The electric field distribution of the mode no. 6 (table 4) with resonant frequency 2.4906 GHz.

Mode no.	Resonant Frequencies (GHz) computed with		Relative difference in percent	Comment
	MAFIA	MWST		
1	1.3079	1.3020	0.45	Operating mode
2	1.7692	1.7565	0.72	
3	1.8337	1.8214	0.68	Degenerate mode (2 fold)
4	1.8736	1.8612	0.66	Degenerate mode (2 fold)
5	1.9281	1.9134	0.77	
6	1.9884	1.9731	0.78	
7	2.0782	2.0647	0.65	
8	2.2387	2.2420	0.14	Degenerate mode (2 fold)
9	2.3422	2.3398	0.10	Degenerate mode (2 fold)
10	2.4906	2.4860	0.19	
11	2.5482	2.5499	0.07	
12	2.7215	2.7216	0.004	
13	2.7249	2.7447	0.72	Degenerate mode (2 fold)
14	2.9994	2.9960	0.11	

Table 5: The resonant frequencies of all the modes bellow the cutoff frequency of the beam pipe computed with MAFIA and Microwave studio.

3.3 Time domain analysis

3.3.1 Scattering Parameters

For the time domain computations the cavity has been modeled as a six-port device. Due to its symmetry, only one quarter of it was modeled. Among the six ports, four are the coaxial ports to be connected to the amplifiers and external loads. The other two ports are waveguide ports due to the beam pipe. The modeled geometry is shown in Fig. 15, along with the relevant coordinate system and the ports assignment. Half of the geometries of the four coaxial ports are visible in the figure. The cutoff frequencies of the first five TM modes of the beam pipe are listed in Table 6. It can be noted here that the operating frequency of the feedback cavity is 1.3079 GHz, which is well below the cutoff frequency of the beam pipe. So, there should be no influences of the beam pipe on the kicker performances in the desired frequency band. For the scattering parameter computations, the structure has been excited with a Gaussian Pulse through the coaxial port 1. All the other ports have been terminated with their corresponding wave impedances. The comparison of the amplitude and phase of the reflection coefficient at port 1 computed with MAFIA and MWST are shown in Fig. 16. The same for the transmission coefficient from port 1 to port 2 are shown in Fig. 17. The agreement between the results from the two codes confirms the consistency in modeling the structure with both the softwares. To verify the point of coupling of the higher order modes of the beam pipe, the same time domain analysis has been done with electric short circuits at the both beam pipes. But no significant difference in the results could be found, which confirms that there are no coupling between the beam pipe and the cavity in that frequency range. It may be noted here that the whole structure has been considered as lossless and the automesh facility has been used for the MWST simulations. In case of the MAFIA computations, a manual meshing has been used. The difference between the two meshing schemes can be the cause of the slight difference of the computed results.

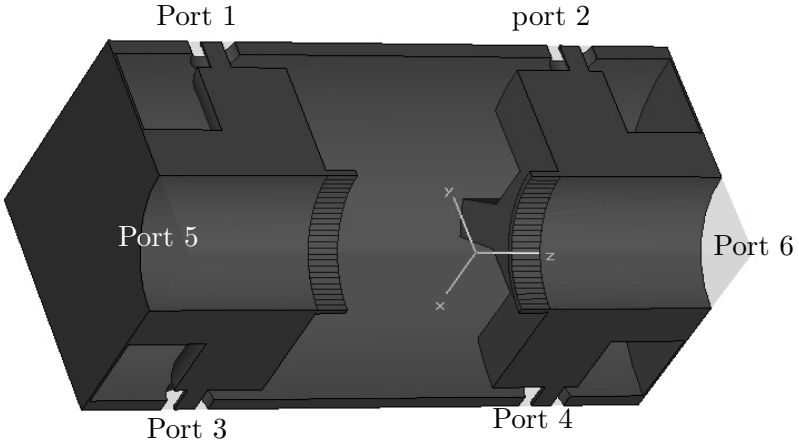

Figure 15: One quarter of the PETRA III longitudinal feedback cavity with the relevant coordinates and the assigned ports.

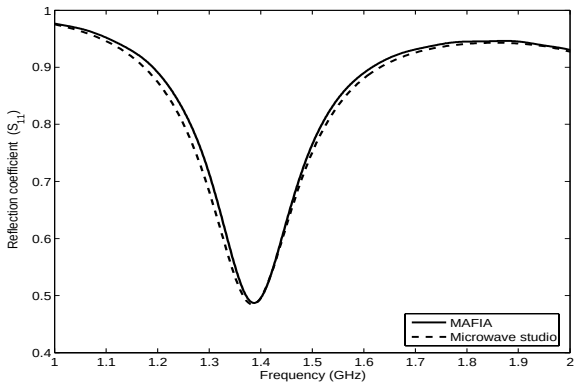

(a) Amplitude of the reflection coefficient at port 1.

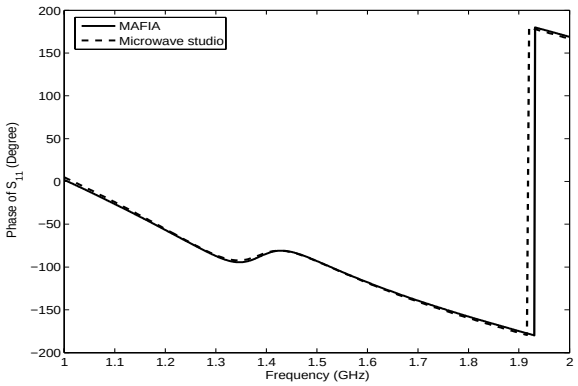

(b) Phase of the reflection coefficient at port 1.

Figure 16: Amplitude and phase of the reflection coefficient at port 1.

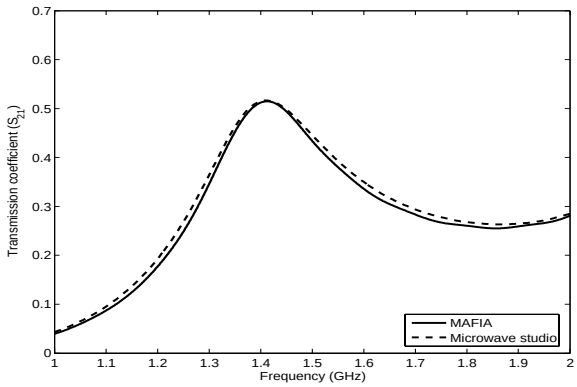

(a) Amplitude of the transmission coefficient from port 1 to port 2.

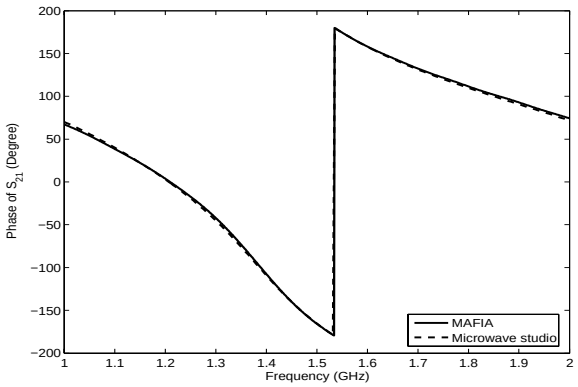

(b) Phase of the transmission coefficient from port 1 to port 2.

Figure 17: Amplitude and phase of the transmission coefficient from port 1 to port 2.

Mode Number	Cutoff frequency (GHz) Microwave Studio	Cutoff frequency (GHz) MAFIA
1	3.822	3.829
2	4.852	4.852
3	8.12	8.174
4	8.42	8.443
5	8.73	8.789

Table 6: Cutoff frequencies of the first five TM waveguide modes of the PETRA III longitudinal feedback cavity beam pipe computed with MWST and MAFIA.

3.3.2 Wake computations with on-axis beam

The time domain wake computations have been done for the feedback cavity with an uniform mesh step size of 0.77 mm along the z-axis. This is a compromise between the available computer memory and the necessity to model the small details of the cavity geometry. A beam with an rms bunch length (σ_z) of 10 mm, traversing the feedback cavity on axis, has been used as the excitation source. The #1dcurrent section of the MAFIA module T3 has been used to define the properties of the exciting beam. A Gaussian charge distribution with a total charge of 1 C has been used. A wakefield monitor has been placed at $x = y = 0$ to record the wakefields as a function of the bunch coordinate (s). The z-component of the wake potential (longitudinal wake) and the bunch charge density versus the bunch coordinate are shown in

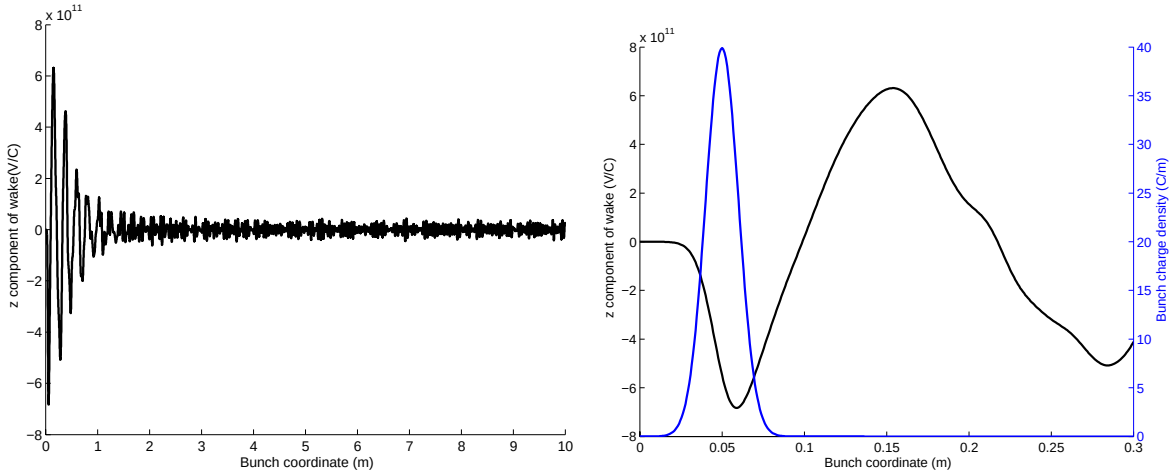

(a) Longitudinal (z) component of the wake for PETRA III feedback cavity along 10 meters of the bunch coordinate.

(b) Longitudinal (z) component of the wake for PETRA III feedback cavity and the bunch charge distribution along 0.3 meters of the bunch coordinate.

Figure 18: Longitudinal component of the wake along the bunch coordinate.

Fig. 18. Fig. 18(b) shows the variation of the longitudinal wake potential and the bunch charge density along 0.3 meter of the bunch coordinate. Fig. 18(a) shows the variation of the wake along 10 meters of the bunch coordinate. The wakes were recorded for such a long time to have enough resolution in the impedance spectrum. The longitudinal loss parameter and the $k(1)$ parameter computed according to the equations 6 and 7 come out to be -4.6997×10^{11} V/C and 1.7489×10^{13} V/(C m), respectively.

In order to compute the impedances of the cavity in frequency domain, a discrete Fourier transform (DFT) has been applied to the longitudinal wakes (shown in Fig. 18). The obtained impedance spectra has been normalized to the bunch spectrum. Fig. 19 shows the longitudinal impedance spectrum of the feedback cavity. The longitudinal impedance spectra of the feedback cavity without the nose cones can be seen in the figure 20. From the figure, it can be noticed that the impedance peak occurs at a bit higher frequency (at 1.49 GHz) with a smaller impedance value. Under the cutoff frequency of the beam pipe some impedance peaks are visible due to the resonant modes of the cavity. Above the cut off of the beam pipe more or less continuous spectra has been obtained which are due to the modes of the beam pipe. From the plot, it may be noticed that the frequency of the first peak (corresponding to the operating mode of the cavity) is 1.379 GHz. This is a bit higher than the computed resonant frequency of the cavity fundamental mode (Table 4). The reason for the difference is, for the eigenmode computations the coaxial ports of the cavity have been treated as short circuited. On the other hand, for the time domain wake computations they have been terminated with corresponding matched termination. Besides the peak due to the fundamental cavity mode, presence of another impedance peak at 2.278 GHz can be noticed. The output wave amplitudes recorded at ports 1 and 2 are shown in Fig. 21. As the beam has been launched from the

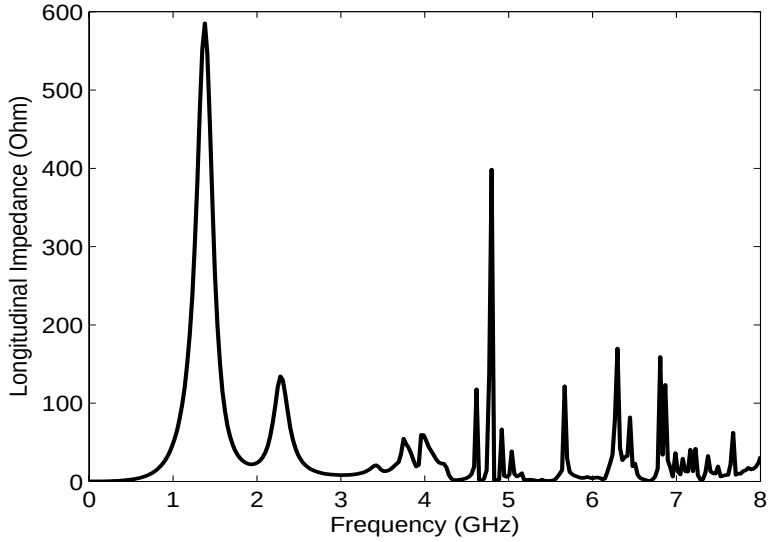

Figure 19: Longitudinal impedance versus frequency for the longitudinal feedback cavity. The coaxial ports are terminated with matched terminations.

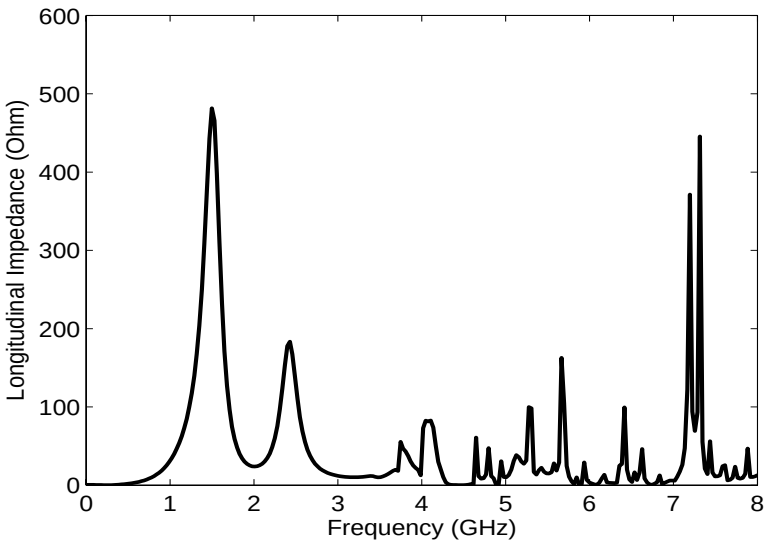

Figure 20: Longitudinal impedance versus frequency for the longitudinal feedback cavity without the nose cones. The coaxial ports are terminated with matched terminations.

left hand side, which is nearer to the port 1, the recorded wave amplitude at port 1 becomes non-zero at first. Due to the symmetry of the cavity, the output signals recorded at ports 3 and 4 are exactly same as those recorded at port 1 and 2.

To investigate the influences of the coaxial port terminations on the wakes and corresponding impedance spectra, the wake computations were repeated with short circuits to all the coaxial ports. All the other simulation parameters except the coaxial port terminations have been kept unchanged. The resulting longitudinal wakes along the bunch coordinate is shown in Fig. 22. As in the previous plot, the variation of the wake potential along 10 m of the bunch coordinate is shown in Fig. 22(a). Fig. 22(b) shows the details of the short range wake along with the bunch charge density at the beginning of the bunch coordinate. The effect of matched terminations at the coaxial waveguide ports are clearly noticeable if we compare the variation of the wakes as plotted in Fig. 18(a) and Fig. 22(a). The corresponding longitudinal impedance spectrum is plotted in Fig. 23. As compared to the previous impedance spectrum, the impedance peaks are much higher and sharp. The impedance peak corresponding to the fundamental cavity mode now appears at 3.19 GHz which is closer to the frequency of the same mode found by the eigenmode analysis. It may be noted here that although the coaxial ports have been terminated with short circuits, the two ports due to the beam-pipes (ports 5 and 6) have still been considered as waveguide ports to allow the excitation beam. Therefore, all the boundary conditions of the cavity in this case are not completely identical with those considered during the eigenmode computations. Impedance peaks at 1.77 GHz, 2.07 GHz and 2.488 GHz (corresponding to the modes no. 2, 7 and 10 of Table 5 respectively) appear in the impedance spectra, which were absent in the impedance spectra with the coaxial ports matched.

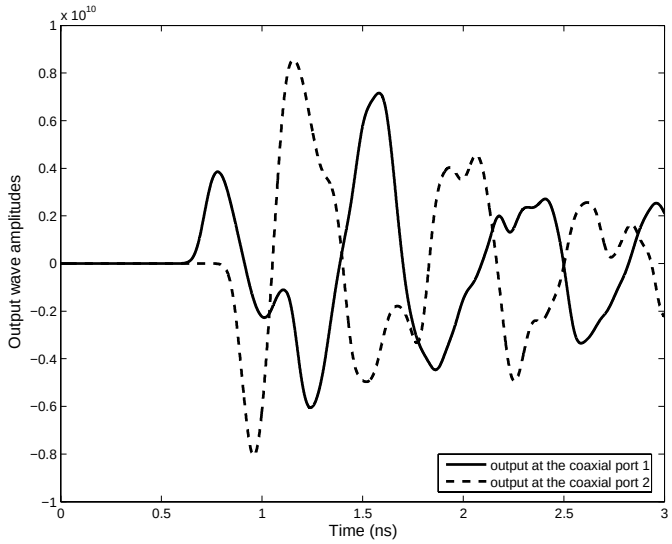

Figure 21: Output wave amplitudes at ports 1 and 2 during the wakefield computation.

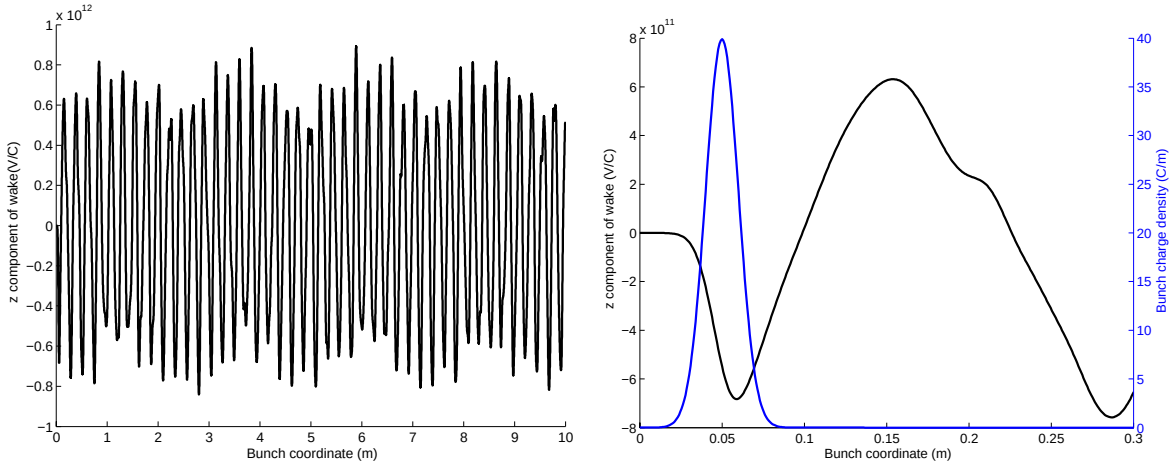

(a) Longitudinal (z) component of the wake for the PETRA III feedback cavity along 10 meters of the bunch coordinate with the coaxial ports terminated with short circuits.

(b) Longitudinal (z) component of the wake for the PETRA III feedback cavity and the bunch charge distribution along 0.3 meters of the bunch coordinate with the coaxial ports terminated with short circuits.

Figure 22: Longitudinal component of the wake along the bunch coordinate with short circuited coaxial ports.

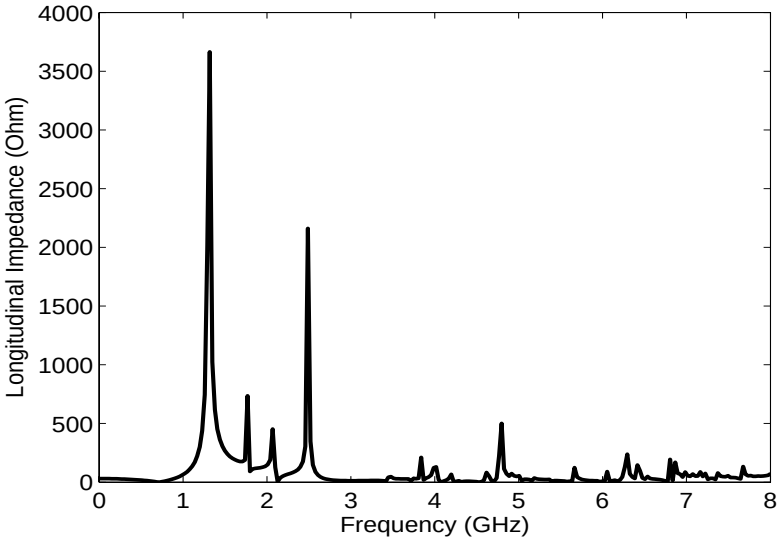

Figure 23: Longitudinal impedance versus frequency for the longitudinal feedback cavity with coaxial ports terminated with short circuits.

3.3.3 Wake computations with off-axis beam

To compute the transverse kick parameters and impedances, the transverse wake components are required. This requires excitation of the cavity with an off-axis beam. For these computations, the method described in section 2.3.2 has been used. A beam with 2 mm offset

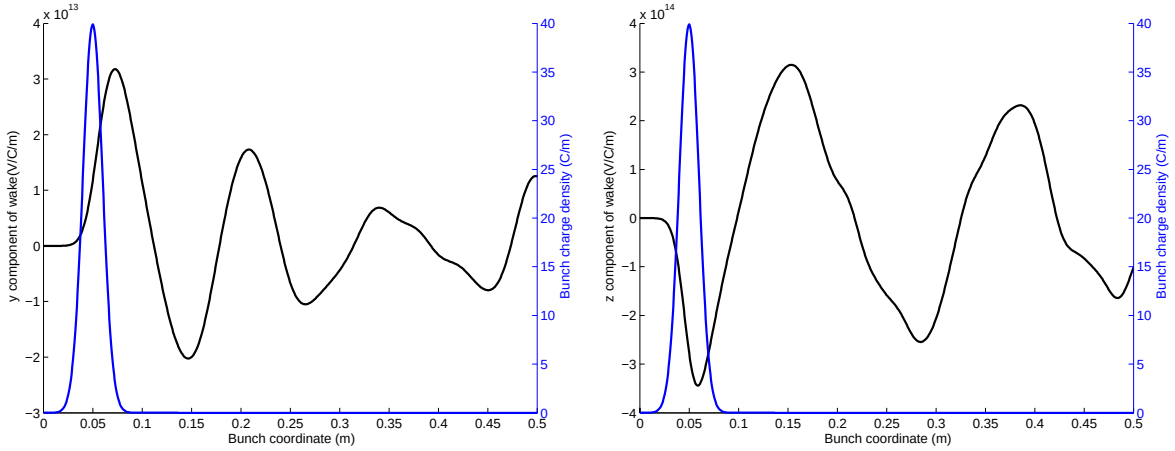

(a) Longitudinal (z) component of the wake normalized to the beam offset.

(b) Transverse (y) component of the wake normalized to the beam offset.

Figure 24: Longitudinal and transverse component of the wake normalized to the beam offset for the PETRA III feedback cavity.

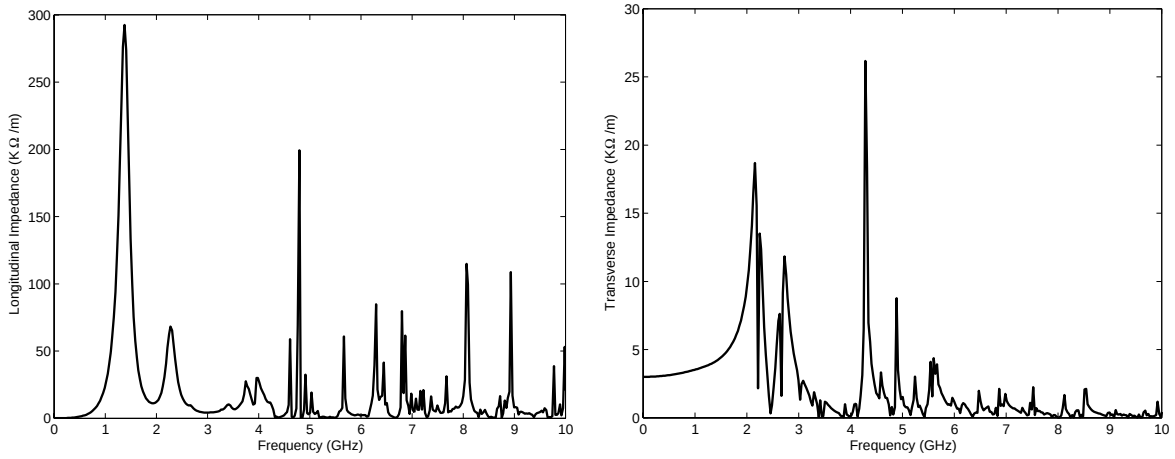

(a) Longitudinal (z) impedance normalized to the beam offset.

(b) Transverse (y) impedance normalized to the beam offset.

Figure 25: Longitudinal and transverse impedances normalized to the beam offset for the PETRA III feedback cavity.

in the y-direction has been used as the excitation source, while the other parameters of the beam were same as before. Fig. 24 shows the longitudinal and transverse components of the wake potential along the bunch coordinate normalized to the beam offset. It may be noted here that for transverse wake computations, all the coaxial ports have been terminated with matched terminations. The longitudinal and transverse impedance normalized to the beam offset is shown in Fig. 25. In the transverse impedance spectra, impedance peaks are visible at the frequencies 2.16 GHz, 2.25 GHz, 2.64 GHz, 2.73 GHz. The impedance peak at 2.25 GHz corresponds to the resonant frequency of the mode no. 8 and that at 2.73 GHz corresponds to the resonant frequency of the mode nos. 12 and 13 of Table 5. The longitudinal loss parameter and $k(1)$ parameter computed according to the equations 6 and 7 for the 2.0 mm offset beam comes out to be -4.7400×10^{11} V/C and 1.7195×10^{13} V/(C m), respectively. Corresponding transverse kick parameter (normalized to the beam offset) computed according to the equation 8 is 1.3150×10^{13} V/(C m). All the loss and kick parameters are summarized in Table 7.

Longitudinal loss parameter [V/C]	$k(1)$ parameter [V/(C m)]	Transverse kick parameter [V/(C m)]
-4.6997×10^{11}	1.7489×10^{13}	n.a.
-4.7400×10^{11} (offset = 2.0 mm)	1.7195×10^{13} (offset = 2.0 mm)	1.3150×10^{13}

Table 7: The loss and kick parameters for the PETRA III longitudinal feedback cavity with nose cones.

All the loss and kick parameters for the same feedback cavity without the nose cones

have also been evaluated. No significant changes have been noticed in the corresponding parameters. For the shake of comparison those parameters are also shown in the Table 8.

Longitudinal loss parameter [V/C]	$k(1)$ parameter [V/(C m)]	Transverse kick parameter [V/(C m)]
-4.5244×10^{11}	1.4127×10^{13}	n.a.
-4.5507×10^{11} (offset = 2.0 mm)	1.3882×10^{13} (offset = 2.0 mm)	1.0723×10^{13}

Table 8: The loss and kick parameters for the DESY longitudinal feedback cavity without nose cones.

3.3.4 Shunt impedances

For the shunt impedance computations, the MAFIA T3 module has been used as described in the section 2.3.3. The correction signal to the beam is to be applied through one of the coaxial ports. Therefore, it is of interest to plot the variation of the electric field along the cavity axis with time corresponding to an excitation through a coaxial port. Fig. 26 shows the variation of the longitudinal electric field along the cavity axis with time. The longitudinal electric field has been shown along the vertical axis (along z), whereas the distance along the cavity axis and the time have been plotted along the x and the y axes respectively. The color-bar represents the strength of the electric field component.

Two sets of computation runs have been done, one for the forward wave case and the other one is for the backward wave case. For the forward wave case, the excitation signal is fed through the one of the upstream coaxial ports, while keeping all the other ports matched. As the beam pipe is circular, it is sufficient to use one coaxial port for the excitations. Fig. 27 shows the variations of computed forward and backward wave shunt impedances for the feedback cavity. From the plot, it can be noticed that the maximum of the shunt impedances occur around 1.38 GHz with a maximum value of 1282 Ω (for the forward wave). Both the forward and the backward wave shunt impedances are a bit lower than those of ELETTRA/SLS kicker [17]. It may be noted here that for the shunt impedance computations, all the coaxial ports have been terminated with corresponding matched terminations. The shunt impedance value may be increased further by applying short circuits at some of the coaxial ports. Another interesting point is to study the effect of the nose cones on the shunt impedances. To appraise this point, the same computations have been carried out for the feedback cavity without the nose cones. The computed shunt impedances are shown in Fig. 28. From Figs. 27 and 28, it is clear that the inclusion of the nose cones have improved the shunt impedances about 13%. The frequency corresponding to the peak of the shunt impedance have also been increased (1.495 GHz) compared to that with the nose cones (1.38 GHz). The maximum value of the forward wave shunt impedance without nose cones comes out to be 1134 Ω.

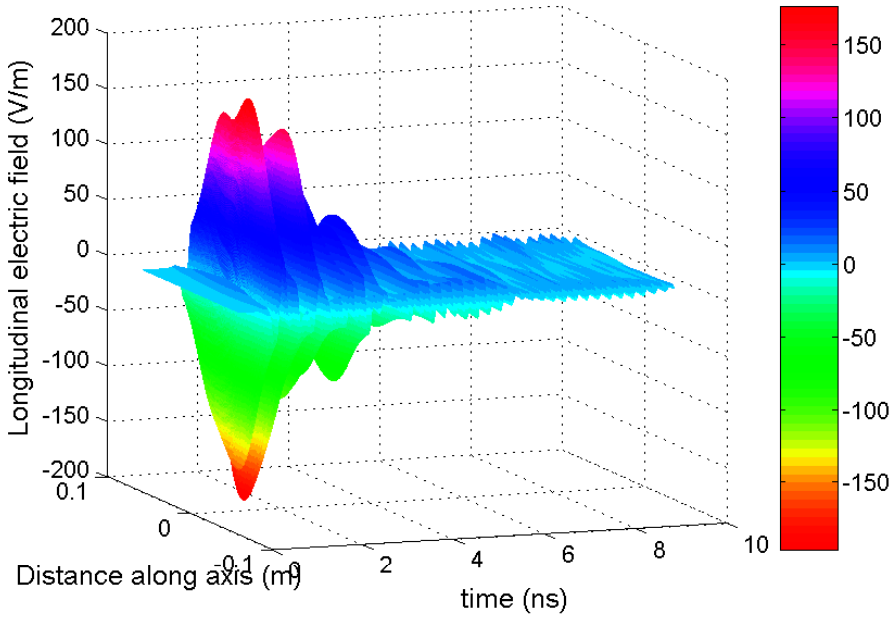

Figure 26: Variation of the longitudinal electric field along the feedback cavity axis with time.

4 Summary

The wakes and impedances computation results for the PETRA III longitudinal feedback cavity have been presented. Both on- and off-axis wakes and related loss and kick parameters

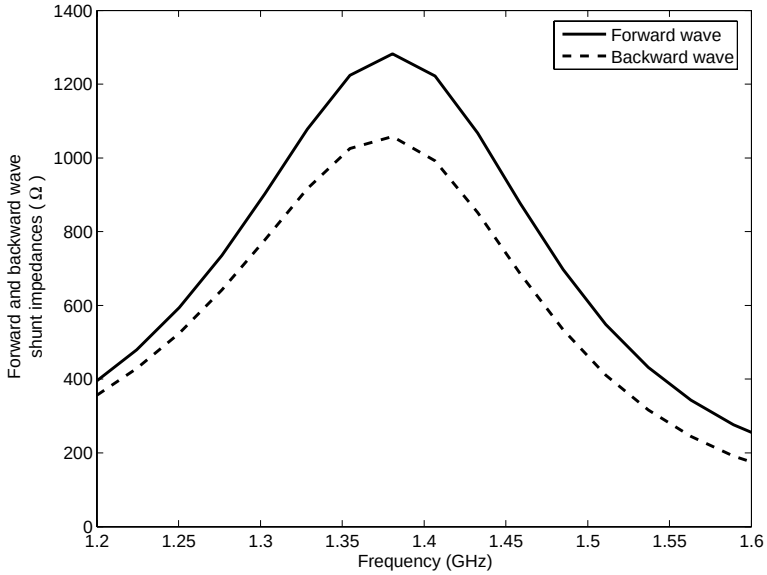

Figure 27: Forward and backward wave shunt impedances for the feedback cavity with the nose cones.

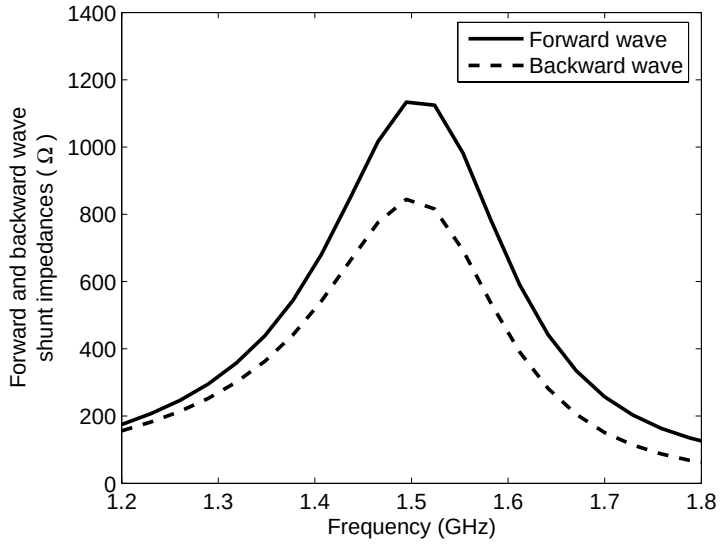

Figure 28: Forward and backward wave shunt impedances for the feedback cavity without the nose cones.

have been estimated. Modal analysis have also been done in order to supplement the time domain wake computation results. The effect of inclusion of the 'nose cones' on the resonance frequency of the operating mode has been pointed out. The effect of the coaxial port terminations on the wakes and impedances of the cavity have been studied. It has been confirmed through simulations that the inclusion of nose cones should increase the corresponding shunt impedance without any significant adverse effect on the cavity performance.

Acknowledgments

We would like to thank Micha Dehler for detailed information about the SLS feedback cavity. Thanks go also to Michael Ebert and Cornelius Martens who designed the DESY version of the feedback cavity and supported us with technical drawings.

References

[1] T. Weiland and R. Wanzenberg, "Wakefields and impedances." Joint US-CERN particle accelerator school, Hilton Head Island, SC, USA, November 1990. Edited by M. Dienes, M. Month and S. Turner.

[2] A. Chao, *Physics of Collective Beam Instabilities in High Energy Accelerators*. New York: John Wiley and Sons, 1993.

[3] P. Wilson, "Introduction to wakefields and wake potentials." U.S. Particle Accelerator School, Batavia, Illinois, July-August 1987.

[4] B. Zotter and S. Kheifets, *Impedances and Wakes in High Energy Particle Accelerators*. London: World Scientific, 1998.

[5] T. Weiland, "Parasitic energy loss due to cavities in PETRA." Internal Report M-81/04, DESY, 1981.

[6] T. Weiland, "PETRA's impedance." Internal Report M-81/23,DESY,1981.

[7] K. Balewski, "Analyse der transversalen Moden-Kopplungsinstabilität für lokalisierte HF-Strukturen und ihre Kompensierbarkeit durch Rückkopplungssysteme." DESY 89-108, Aug. 1989.

[8] K. Balewski, W. Brefeld, W. Decking, H. Franz, R. Röhlsberger, E. Weckert, Eds., "PETRA III: A low emittance synchrotron radiation source." Technical Design Report, DESY 2004-035, February 2004.

[9] T. Weiland, "On the computation of resonant modes in cylindrically symmetric cavities," *Nuclear Instruments and Methods*, vol. 216, pp. 329–348, 1983.

[10] "CST microwave studio, version 5." http://www.cst.com, March 2005. CST GmbH.

[11] "MAFIA, release 4." http://www.cst.com, Nov 2004. CST GmbH.

[12] P. Wilson, "High-energy electron linacs: Applications to storage ring RF systems and linear colliders," *AIP Conf. Proc.*, vol. 87, pp. 450–555, 1982.

[13] "MATLAB, version 7.0." http://www.mathworks.com, 2005. The MathWorks Inc.

[14] J. Corlett, J. Johnson, G. Lambertson, and F. Voelker, "Longitudinal and transverse feedback kickers for ALS," in *4th European Particle Accelerator Conference (EPAC)*, (London), pp. 1625–1627, June 1994.

[15] R. Boni, A. Gallo, A. Ghigo, F. Marcellini, M. Serio, and M. Zobov, "A waveguide over-loaded cavity as longitudinal kicker for the DAFNE bunch-by-bunch feedback system," *Particle Accelerators*, vol. 52, pp. 95–113, 1996.

[16] L. Chang, W. Lau, and T. Yang, "Development of the RF kicker for the longitudinal feedback system at SRRC," in *6th European Particle Accelerator Conference (EPAC)*, (Stockholm), pp. 1708–1710, June 1998.

[17] M. Dehler, "Kicker design for the ELETTRA/SLS longitudinal multi-bunch feedback," in *8th European Particle Accelerator Conference (EPAC)*, (Paris, France), pp. 2070–2072, 2002.